

# An efficient, tunable and robust source of narrow-band photon pairs at the Rubidium D1 line

Janik Wolters,<sup>1, 2, a)</sup> Roberto Mottola,<sup>1</sup> Chris Müller,<sup>3</sup> Gianni Buser,<sup>1</sup> Tim Kroh,<sup>3</sup> Andreas Ahlrichs,<sup>3</sup> Sven Ramelow,<sup>3, 4</sup> Oliver Benson,<sup>3, 4</sup> and Philipp Treutlein<sup>1</sup>

<sup>1)</sup>Departement Physik, Universität Basel, Klingelbergstr. 82, 4056 Basel, Switzerland.

<sup>2)</sup>Deutsches Zentrum für Luft- und Raumfahrt e.V. (DLR), Institute of Optical Sensor Systems, Rutherfordstr. 2, 12489 Berlin, Germany.

<sup>3)</sup>Institut für Physik, Humboldt-Universität zu Berlin, Newtonstr. 15, 12489 Berlin, Germany.

<sup>4)</sup>IRIS Adlershof, Humboldt-Universität zu Berlin, Zum Großen Windkanal 6, 12489 Berlin, Germany.

(Dated: 21 December 2024)

We present an efficient, bright, and robust source of photons at the rubidium D1-line (795 nm) with a narrow bandwidth of  $\delta = 226(1)$  MHz. The source is based on non-degenerate, cavity-enhanced spontaneous parametric down-conversion in a monolithic optical parametric oscillator far below threshold. The setup allows for efficient coupling to single mode fibers. A heralding efficiency of  $\eta_{\text{heralded}} = 45(5)$  % is achieved, and the uncorrected number of detected photon pairs is  $3.8 \times 10^3$  cts/(s mW). For pair generation rates up to 0.5 MHz, the source emits heralded single photons with negligible contamination from higher photon number states as evidenced by  $g_c^{(2)} < 0.01$ . The source is intrinsically stable due to the monolithic configuration. Frequency drifts are on the order of  $\delta/20$  per hour even without active stabilization. By applying mechanical strain, the source frequency can be fine-tuned within a range of  $\geq 2$  GHz.

## I. INTRODUCTION

Photonics is among the most promising platforms for realizing quantum technology, in particular quantum communication networks, quantum simulators, and quantum computers. Research is driven by manifold benefits: quantum repeater networks promise unconditional secure communication<sup>1–3</sup>, quantum simulators further better understanding of complex quantum systems, e.g. in chemistry or many-body physics<sup>4–7</sup>, and quantum computers promise exponential speed-up in solving complex problems<sup>8–10</sup>.

To realize these applications, excellent single-photon sources are required. Ideally, such single-photon sources emit one photon at a time, on demand, at a high generation rate, and in a pure state of a single spatial, temporal, and spectral mode. Moreover, each copy of such a source should be capable of generating photons identical to those stemming from the others<sup>11</sup>. Current sources can only fulfill a limited number of the above requirements while maintaining high performance for specific applications. Among the most advanced single photon sources are semiconductor quantum dots<sup>12–16</sup> and sources based on spontaneous parametric down conversion (SPDC)<sup>17–21</sup>. Currently, the latter offer three major advantages: reproducibility of their construction, room temperature operation, and perfectly indistinguishable photons. The final point is demonstrated by observations of high visibility quantum interference of photon pairs from different sources<sup>22</sup>.

Despite these features, a major drawback of SPDC sources is the intrinsically probabilistic photon generation with a photon generation probability  $\epsilon \ll 1$  per coherence time. When  $N$  photons are needed simultaneously to feed a quantum photonic circuit, the success probability scales exponentially as  $P \sim \epsilon^N$ . In typical state-of-the-art experiments, five-photon events occur at rates below 1 Hz,<sup>23</sup> and ten-photon events are observed every few hours.<sup>24</sup> This problem can be circumvented by massive multiplexing<sup>25–29</sup> or by combining a heralded source with a memory that can store and release photons in a controlled way<sup>30–34</sup>. Suitable atomic memories have been pushed forward in recent years<sup>35–37</sup>, but require SPDC sources with compatible bandwidths on the order of 1 GHz.

SPDC sources are based on optical second-order nonlinearities ( $\chi^{(2)}$ ) in dielectric media. In this process photons with pump frequency  $\omega_p$  are converted into signal-idler pairs with frequencies  $\omega_s$  and  $\omega_i$  respectively, whereby photon momentum must be conserved (phase matching). To generate signal and idler photons in co-propagating modes quasi-phase matching is achieved by periodic poling of the medium. Typical poling periods are on the order of 10  $\mu\text{m}$ , and high uniformity can be maintained over a few centimeters. This leads to forward emission with a signal/idler spectral bandwidth of a few 100 GHz. The generated light couples well to fibers, leading to heralding efficiencies  $> 90$  % for a fiber coupled source<sup>38</sup>, or  $> 50$  % for a fiber pigtailed source<sup>39</sup>. To efficiently generate photons with a bandwidth between 1 MHz and 1 GHz, i.e. well matched to atomic memory systems, resonator enhanced sources have been developed<sup>17–19</sup>. At their core, these are optical parametric oscillators (OPO),

<sup>a)</sup>Electronic mail: janik.wolters@dlr.de

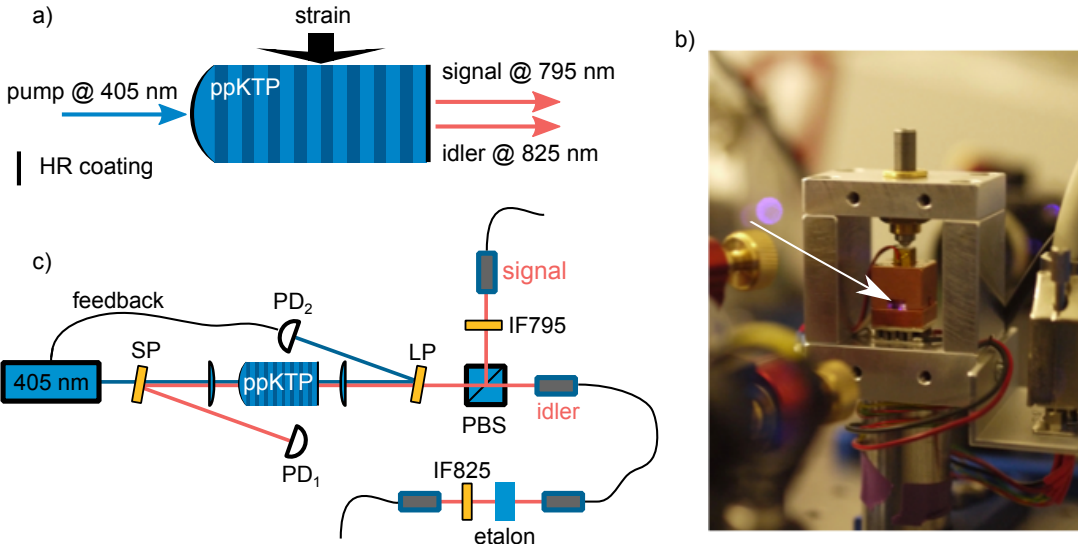


FIG. 1. The experimental setup. a) Sketch of the monolithic OPO that is tuned by applying mechanical strain and controlling the temperature. Highly reflective (HR) coatings are applied on both end facets of the ppKTP crystal to form an optical cavity for the pump, signal, and idler wavelengths. b) Photograph of the oven (housing partially removed) that contains the ppKTP crystal. Mechanical strain can be applied via a fine-threaded screw and piezo. The arrow indicates the position of the ppKTP crystal. c) The optical setup used to pump the OPO and to collect signal and idler photons into optical fibers. SP, LP, IF: short-pass, long-pass, and band-pass interference filters respectively. PD: photodiode. PBS: polarizing beamsplitter.

placed in cavities and pumped far below threshold<sup>40,41</sup>. By increasing the electric field per photon, the triple resonant cavity enhances the generated pair rate per mW of pump power and simultaneously forces the emitted light into narrow spectral lines arranged in clusters<sup>18,20,21,42</sup>.

In this letter, we present a monolithic, cavity-enhanced, non-degenerate SPDC source that generates signal photons at the <sup>87</sup>Rb D1 line (795 nm), with a spectral bandwidth of 226(1) MHz and a heralding efficiency of  $\eta_{\text{heralded}} = 45(5)\%$ . The source can be fine-tuned over a range of  $\geq 2$  GHz by applying mechanical strain. The passive stability is limited by long-term drifts on the order of 10 MHz/h. As such, it is directly compatible with atomic vapor cell quantum memories<sup>35</sup>.

## II. EXPERIMENTAL SETUP

The triple resonant OPO consists of a single periodically poled Potassium Titanyl (ppKTP) crystal (*Raicol Crystals*), sized  $1 \times 2 \times 7$  mm<sup>3</sup>, with a  $10.1 \mu\text{m}$  poling period for type-II conversion of 405 nm pump photons to 795 nm (825 nm) signal (idler) photons. The crystal forms a hemispherical Fabry-Pérot resonator where the spherically convex facet has a 10 mm radius of curvature, see Fig. 1 a. Highly reflective dielectric coatings were applied with nominal reflectivities of  $R_{s/i}^c = 99.9\%$  for the signal/idler and  $R_p^c = 90\%$  for the pump wavelength on the convex facet, and  $R_{s/i}^p = 91.5\%$  and  $R_p^p = 99\%$  on the planar facet. Accounting for losses in the material, this allows for critical coupling of the pump light, while virtually all signal and idler photons leave through the planar surface. The crystal is sandwiched between two highly polished copper plates to apply mechanical strain perpendicular to the optical axis for fine-tuning of the triple resonance condition, see Fig. 1 b. Using a thermoelectric element and a digital temperature controller, the mechanical mount is temperature controlled and stabilized to  $\pm 5$  mK. For optical pumping of the OPO, a grating stabilized 405 nm diode laser provides up to 100 mW of optical power.

The transmission peaks of the ppKTP cavity are detected by an amplified photodiode (PD<sub>2</sub> in Fig. 1 c) and used to stabilize the pump laser frequency on the OPO resonances. The signal and idler photons are separated on a polarizing beamsplitter and coupled into polarization maintaining single mode fibers with anti-reflection coated facets. Prior to the detection by avalanche photodiodes (APDs), the signal photons are filtered by a narrow-band (0.4 nm FWHM) interference filter (IF) with  $> 90\%$  transmission, while the idler photons are filtered by a temperature stabilized etalon (FWHM = 350 MHz, FSR = 13 GHz) and an IF with 0.4 nm FWHM. The filtering stage in the idler arm reaches a peak transmission of  $\approx 80\%$ . For adjustment and characterization, a tunable 795 nm diode laser that is referenced to the <sup>87</sup>Rb D1 line can be injected into the OPO via the signal arm to measure the transmission spectrum on PD<sub>1</sub>. The same laser is simultaneously used to stimulate difference frequency generation (DFG) at the idler wavelength as a tool for measuring the spectrum of the OPO. For detecting the DFG signal, an amplified photodiode is inserted into the idler arm prior to the filtering stage.

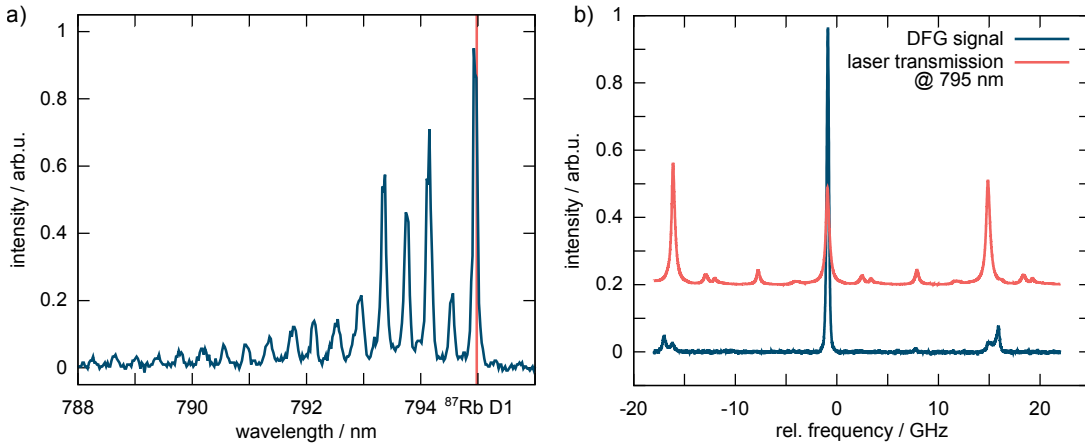


FIG. 2. The spectral properties of the source. a) Spectrum of the signal photons recorded on a sensitive high resolution spectrometer after coarse tuning. The vertical red line indicates the position of the  $^{87}\text{Rb}$  D1 line at 794.979 nm. b) Transmission spectrum of the ppKTP cavity around the  $^{87}\text{Rb}$  D1 line, recorded on  $\text{PD}_1$  and the corresponding DFG intensity measured simultaneously on an amplified photodiode in the idler arm. In the 795 nm laser transmission, three major peaks corresponding to the  $\text{TEM}_{00}$  modes of the cavity are visible. The free spectral range (FSR) is 16 GHz. The DFG signal shows the fine structure of one emission cluster and consists of a central peak accompanied by two weaker doublets separated by one FSR. Outside the displayed frequency window no DFG signal was measurable.

### III. RESULTS

For coarse adjustment of the signal frequency the IF is removed and a spectrum of the signal photons is recorded using a 500 mm grating spectrometer with a sensitive CCD camera. The signal spectrum (Fig. 2 a) spans across the phase matching bandwidth of a few nm and shows several sharp lines separated by 0.5 nm. Each line corresponds to one emission cluster. The fine structure of the individual clusters is not resolved. The wavelength of the brightest cluster at the red side of the spectrum is tuned to be in close proximity to the  $^{87}\text{Rb}$  D1 line by adjusting the crystal temperature and pumping wavelength. Subsequently, the OPO is seeded by the tunable 795 nm laser. This allows to measure the OPO transmission, as well as to record the intensity of the DFG signal while the tunable laser is scanned by  $\pm 20$  GHz around the  $^{87}\text{Rb}$  D1 transitions, see Fig. 2 b. By this the fine structure of the emission cluster is measured. Due to the large free spectral range (FSR) of the OPO cavity, the cluster consists of one strong central peak for which signal and idler resonances are perfectly aligned and two weaker doublet peaks. Since the pump is locked to the cavity resonance, perfect triple resonance is achieved at the central mode. The central peak has a bandwidth of  $\delta = 226(1)$  MHz (FWHM), determined by the finesse and FSR of the ppKTP cavity. Due to the comparably large finesse, the central peak contributes 75 % to the overall intensity of the cluster.

The filtering stage in the idler arm is adjusted to transmit the central DFG peak. Subsequently, the seeding laser is switched off and single photons in the signal and idler arms are measured by time-tagged time-resolved (TTTR) photon counting. At a pump power of  $P_{\text{pump}} = 1.2$  mW, we typically detect photons in the signal and idler arm at a rate of  $n_s = 57 \times 10^3$  cts/(s mW) and  $n_i = 14 \times 10^3$  cts/(s mW), normalized to  $P_{\text{pump}}$  respectively. The idler rate is lower due to more stringent spectral filtering and higher losses compared to the signal arm. The second-order cross-correlation between signal and idler  $g_{s,i}^{(2)}(0) \gg 2$  shows pronounced super-thermal bunching for zero time delay, see Fig. 3(a). This is a first indication of the generation of non-classical light. Integrating the total number of coincidences within  $\Delta t = 8$  ns around the detection time of the idler photon, we obtain the detected signal-idler pair rate  $r = 3.8 \times 10^3$  cts/(s mW), normalized to  $P_{\text{pump}}$ . Correcting for the detector efficiency of  $\eta_{\text{det}} = 60(6)$  %, we estimate the efficiency of the signal arm to be  $\eta_{\text{heralded}} = \frac{r}{\eta_{\text{det}} n_i} = 45(5)$  %. Up to  $\eta_{\text{heralded}} = 50(5)$  % has been observed, i.e. detection of an idler photon indicates the presence of a signal photon in the polarization maintaining single mode fiber with a probability of about 1/2. By improving on the surface quality of the ppKTP crystal, the dielectric coatings, and the collection optics the efficiency will be pushed further towards unity in future experiments. The total rate of generated photon pairs, normalized to  $P_{\text{pump}}$ , is  $R = n_i n_s / r = 210 \times 10^3$  cts/(s mW).

To estimate the purity of the heralded single photons, i.e. the degree of contamination with higher photon number states, we measured the time integrated second-order autocorrelation  $g_c^{(2)}$  conditioned on the detection of an idler photon. To this end, we performed TTTR photon counting with three detectors: two ( $\text{APD}_1$  and  $\text{APD}_2$ ) in Hanbury Brown and Twiss configuration in the signal arm, and one ( $\text{APD}_3$ ) in the idler arm. From the measured detection rates in the TTTR-data we estimated the single photon probability  $P_{s_1}$  ( $P_{s_2}$ ) for detection of one signal photon on  $\text{APD}_1$  ( $\text{APD}_2$ ) within a coincidence window of  $\Delta t = 8$  ns upon the detection of an idler photon, as well as the two photon probability  $P_d$  to detect two signal photons upon the detection of an idler photon. From this, the measured conditional second-order autocorrelation  $g_c^{(2)} = P_d / (P_{s_1} P_{s_2})$  is computed. Assuming a linear

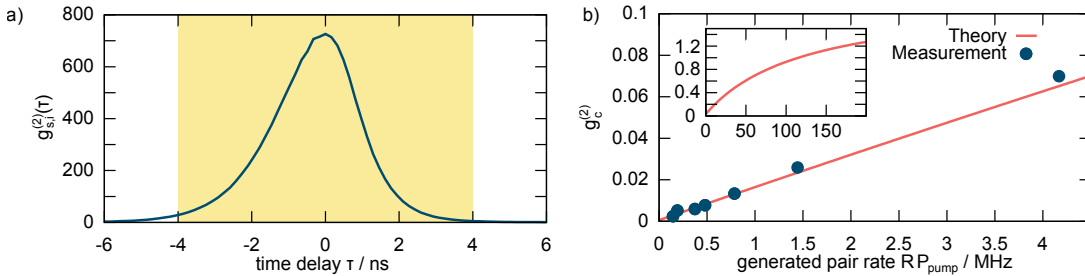


FIG. 3. Second order correlations of the generated photons. a) Measured second-order cross-correlation between signal and idler photons  $g_{s,i}^{(2)}(\tau)$ . The pronounced bunching at zero time delay indicates that photons are emitted in pairs. The yellow shaded area indicates the coincidence window with  $\Delta t = 8$  ns used for evaluating the second order correlation shown in b). The temporal asymmetry reflects the dissimilar frequency filtering in signal and idler arms. b) Conditional second-order autocorrelation  $g_c^{(2)}$  for various pair generation rates. The source emits single photons with a purity  $g_c^{(2)} < 0.01$  for generation rates up to 0.5 MHz. The inset shows the theoretical curve for  $g_c^{(2)}$  for generation rates of up to 200 MHz, approaching  $g_c^{(2)} = 2$ , i.e. thermal emission at infinite generation rates.

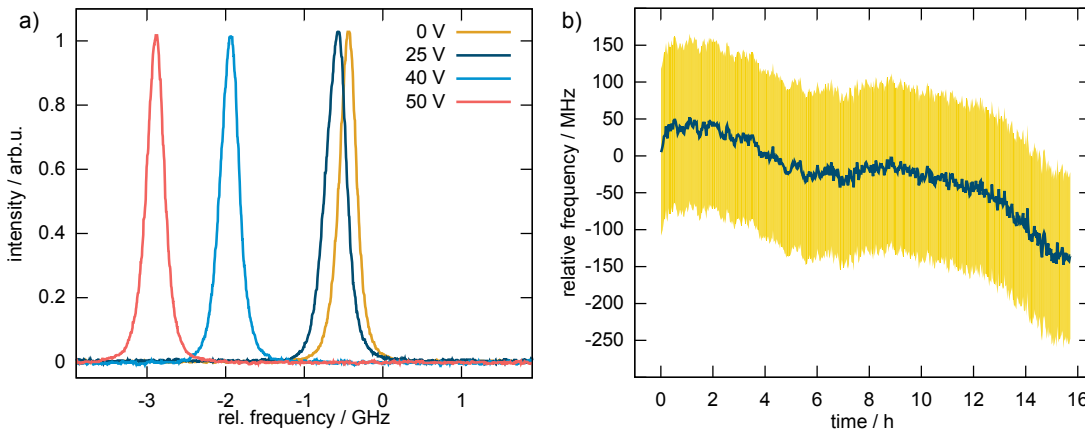


FIG. 4. Tuning behaviour and stability of the source. a) Fine-tuning properties of the source. The measured DFG intensity depending on the seeding laser frequency relative to the  $^{87}\text{Rb}$  D1 line is shown for various piezo voltages. At  $\approx 20$  V the piezo makes contact with the copper stamp and nearly linear tuning of the central emission peak by several GHz can be achieved. b) Measurement of the source stability. While the source temperature is kept constant and the pump laser is stabilized to be on resonance with the OPO, the seeding frequency for maximum DFG signal is measured relative to the initial value (blue curve). The yellow shaded area indicates the FWHM linewidth of the DFG signal. The frequency measurement error is on the order of 5 MHz (error bars not shown for clarity)

relation between photon number and detection probability for  $P_{s1} \ll 1$  we estimate  $P_{s1} \approx P_{s2} \approx \frac{\eta_{\text{heralded}}\eta_{\text{det}}}{2} (1 + P_{\text{pump}}R\Delta t)$ , where the factor 1/2 accounts for the beamsplitter in the HBT setup, the first addend for the heralded signal photon and the second one for additional uncorrelated signal photons emitted within the coincidence window. Similarly,  $P_d \approx P_{s1} \cdot \eta_{\text{heralded}}\eta_{\text{det}}P_{\text{pump}}R\Delta t$ . We find that  $g_c^{(2)}$  as function of the pair generation rate  $R \cdot P_{\text{pump}}$  follows

$$g_c^{(2)} \approx 2 \frac{R \cdot P_{\text{pump}}\Delta t}{1 + R \cdot P_{\text{pump}}\Delta t}. \quad (1)$$

As shown in Fig. 3(b) the measured  $g_c^{(2)}$  perfectly follows the theoretical prediction. For generation rates of up to 0.5 MHz, the source emits single photons with a purity  $g_c^{(2)} < 0.01$ , proving that multi-photon generation is strongly suppressed.

To fine-tune the emission frequency of the source, mechanical strain is applied onto the ppKTP crystal along the vertical axis<sup>43,44</sup>. The strain deforms the refractive index ellipsoid and allows for fine-tuning of the triple resonance condition. To this end, a piezoelectric actuator presses a highly polished copper stamp onto the ppKTP crystal that is lying on a second polished copper surface, see Fig. 1c. By switching on the seeding laser, changing the piezo voltage, and subsequently readjusting the crystal temperature by a few tens of mK to reestablish triple resonance, the signal photon frequency can be tuned by  $\approx -2$  GHz from the initial value, as illustrated in Fig. 4(a). After careful pre-adjustment this is sufficient to reach a desired frequency, e.g. slightly red-detuned from the  $F = 1 \rightarrow F' = 1$  transition of atomic  $^{87}\text{Rb}$ , where EIT quantum memories work preferentially<sup>35,45</sup>.

To evaluate the frequency stability of the OPO, the source was operated continuously for 16 h while seeded by the tunable 795 nm laser. The laser frequency relative to the  $^{87}\text{Rb}$  D1 line was repeatedly scanned, and the frequency corresponding to the maximum DFG signal was recorded, see Fig. 4(b). We measured an average frequency drift of about 10 MHz per hour without any feedback on the emission frequency. It remained possible to reach the  $F = 1 \rightarrow F' = 1$  transition by strain and temperature tuning over a period of several weeks. However, on longer timescales changes of the triple resonance frequencies that could not be compensated by changing the piezo voltage and temperature occurred. We attribute these changes to pump-induced gray tracking<sup>46,47</sup> that affects the cavity modes. When the tuning range is thus exhausted a major readjustment is required to bring the source back within range of the desired atomic transition. Alternatively, the source can be pumped off-resonantly, however this requires larger pumping powers to reach the same pair rate.

#### IV. DISCUSSION

A cavity enhanced narrow-band photon pair source based on a monolithic OPO was presented. The monolithic OPO can be tuned over several GHz, exhibits high stability, and, unlike preceding designs, does not need active stabilization of the OPO cavity. Moreover, intra-cavity surfaces that tend to introduce losses are avoided and consequently a high heralding efficiency of  $\eta_{\text{heralded}} = 45(5)\%$  is reached. Using improved collection optics, potentially comprising adaptive elements<sup>48</sup> and improved dielectric coatings, the heralding efficiency could be further pushed towards unity. Even at comparably high photon pair generation rates of up to  $R = 0.5$  MHz the signal photons show pronounced single photon characteristics with measured  $g_c^{(2)} < 0.01$ . With this the source is directly compatible with atomic vapor based quantum memories<sup>35</sup> that will be used in future experiments to synchronize the probabilistic photon generation. Nearly ideal compound photon sources that emit one photon at a time, on demand, and in a single spatial, temporal, and spectral mode can then be constructed in a reproducible fashion. These have high potential to enable photonic quantum simulation and computing with many photons.

#### V. ACKNOWLEDGMENTS

JW was supported by the Marie Skłodowska-Curie Actions of the EU Horizon 2020 Framework Programme under grant agreement No. 702304 (3-5-FIRST). RM, GB, and PT acknowledge support by the Swiss National Science Foundation through NCCR QSIT. SR was supported by German Research Foundation (DFG) within the Emmy-Noether-Programm (RA 2842/1-1). CM, TK and OB were supported by the German Research Foundation (DFG) Collaborative Research Center (CRC) SFB 787 project C2 and the German Federal Ministry of Education and Research (BMBF) project Q.Link-X.

- <sup>1</sup>N. Sangouard, C. Simon, H. de Riedmatten, and N. Gisin, *Reviews of Modern Physics* **83**, 33 (2011).
- <sup>2</sup>H. J. Kimble, *Nature* **453**, 1023 (2008).
- <sup>3</sup>N. Gisin, G. Ribordy, W. Tittel, and H. Zbinden, *Reviews of Modern Physics* **74**, 145 (2002).
- <sup>4</sup>I. Buluta and F. Nori, *Science* **326**, 108 (2009).
- <sup>5</sup>I. Georgescu, S. Ashhab, and F. Nori, *Reviews of Modern Physics* **86**, 153 (2014).
- <sup>6</sup>M. Reiher, N. Wiebe, K. M. Svore, D. Wecker, and M. Troyer, *Proceedings of the National Academy of Sciences* **114**, 7555 (2017).
- <sup>7</sup>Y. Cao, J. Romero, J. P. Olson, M. Degroote, P. D. Johnson, M. Kieferová, I. D. Kivlichan, T. Menke, B. Peropadre, N. P. D. Sawaya, S. Sim, L. Veis, and A. Aspuru-Guzik, arXiv: , 1812.09976http://arxiv.org/abs/1812.09976v2.
- <sup>8</sup>T. D. Ladd, F. Jelezko, R. Laflamme, Y. Nakamura, C. Monroe, and J. L. O'Brien, *Nature* **464**, 45 (2010).
- <sup>9</sup>P. Kok, W. J. Munro, K. Nemoto, T. C. Ralph, J. P. Dowling, and G. J. Milburn, *Reviews of Modern Physics* **79**, 135 (2007).
- <sup>10</sup>J. L. O'Brien, *Science* **318**, 1567 (2007).
- <sup>11</sup>F. Flaminio, N. Spagnolo, and F. Sciarrino, *Reports on Progress in Physics* **82**, 016001 (2018).
- <sup>12</sup>P. Senellart, G. Solomon, and A. White, *Nature Nanotechnology* **12**, 1026 (2017).
- <sup>13</sup>A. Reigue, J. Iles-Smith, F. Lux, L. Monniello, M. Bernard, F. Margaillan, A. Lemaitre, A. Martinez, D. P. McCutcheon, J. Mørk, R. Hostein, and V. Voliotis, *Physical Review Letters* **118** (2017).
- <sup>14</sup>A. Thoma, P. Schnauber, M. Gschrey, M. Seifried, J. Wolters, J.-H. Schulze, A. Strittmatter, S. Rodt, A. Carmele, A. Knorr, T. Heindel, and S. Reitzenstein, *Physical Review Letters* **116** (2016).
- <sup>15</sup>L. Béguin, J.-P. Jahn, J. Wolters, M. Reindl, Y. Huo, R. Trotta, A. Rastelli, F. Ding, O. G. Schmidt, P. Treutlein, and R. J. Warburton, *Physical Review B* **97** (2018).
- <sup>16</sup>P. Lodahl, *Quantum Science and Technology* **3**, 013001 (2017).
- <sup>17</sup>M. Scholz, L. Koch, and O. Benson, *Physical Review Letters* **102**, 063603 (2009).
- <sup>18</sup>A. Ahlrichs and O. Benson, *Applied Physics Letters* **108**, 021111 (2016).
- <sup>19</sup>J. Fekete, D. Rieländer, M. Cristiani, and H. de Riedmatten, *Physical Review Letters* **110**, 220502 (2013).
- <sup>20</sup>K.-H. Luo, H. Herrmann, S. Krapick, B. Brecht, R. Ricken, V. Quiring, H. Suche, W. Sohler, and C. Silberhorn, *New Journal of Physics* **17**, 073039 (2015).
- <sup>21</sup>C.-S. Chuu, G. Y. Yin, and S. E. Harris, *Applied Physics Letters* **101**, 051108 (2012).
- <sup>22</sup>H. de Riedmatten, I. Marcikic, W. Tittel, H. Zbinden, D. Collins, and N. Gisin, *Physical Review Letters* **92** (2004).
- <sup>23</sup>H.-S. Zhong, Y. Li, W. Li, L.-C. Peng, Z.-E. Su, Y. Hu, Y.-M. He, X. Ding, W. Zhang, H. Li, L. Zhang, Z. Wang, L. You, X.-L. Wang, X. Jiang, L. Li, Y.-A. Chen, N.-L. Liu, C.-Y. Lu, and J.-W. Pan, *Physical Review Letters* **121** (2018).
- <sup>24</sup>L.-K. Chen, Z.-D. Li, X.-C. Yao, M. Huang, W. Li, H. Lu, X. Yuan, Y.-B. Zhang, X. Jiang, C.-Z. Peng, L. Li, N.-L. Liu, X. Ma, C.-Y. Lu, Y.-A. Chen, and J.-W. Pan, *Optica* **4**, 77 (2017).

<sup>25</sup>A. L. Migdall, D. Branning, and S. Castelletto, *Physical Review A* **66** (2002).

<sup>26</sup>J. H. Shapiro and F. N. Wong, *Optics Letters* **32**, 2698 (2007).

<sup>27</sup>N. Sinclair, E. Saglamyurek, H. Mallahzadeh, J. A. Slater, M. George, R. Ricken, M. P. Hedges, D. Oblak, C. Simon, W. Sohler, and W. Tittel, *Phys. Rev. Lett.* **113**, 053603 (2014).

<sup>28</sup>F. Kaneda, B. G. Christensen, J. J. Wong, H. S. Park, K. T. McCusker, and P. G. Kwiat, *Optica* **2**, 1010 (2015).

<sup>29</sup>C. Joshi, A. Farsi, S. Clemmen, S. Ramelow, and A. L. Gaeta, *Nature Commun.* , 847 (2018).

<sup>30</sup>E. Jeffrey, N. A. Peters, and P. G. Kwiat, *New Journal of Physics* **6**, 100 (2004).

<sup>31</sup>T. B. Pittman, B. C. Jacobs, and J. D. Franson, *Physical Review A* **66**, 042303 (2002).

<sup>32</sup>J. Nunn, N. K. Langford, W. S. Kolthammer, T. F. M. Champion, M. R. Sprague, P. S. Michelberger, X.-M. Jin, D. G. England, and I. A. Walmsley, *Physical Review Letters* **110**, 133601 (2013).

<sup>33</sup>X.-L. Pang, A.-L. Yang, J.-P. Dou, H. Li, C.-N. Zhang, E. Poem, D. J. Saunders, H. Tang, J. Nunn, I. A. Walmsley, and X.-M. Jin, *arXiv* , 1803.07122http://arxiv.org/abs/1803.07122v1.

<sup>34</sup>F. Kaneda, F. Xu, J. Chapman, and P. G. Kwiat, *Optica* **4**, 1034 (2017).

<sup>35</sup>J. Wolters, G. Buser, A. Horsley, L. Béguin, A. Jöckel, J.-P. Jahn, R. J. Warburton, and P. Treutlein, *Physical Review Letters* **119**, 060502 (2017).

<sup>36</sup>K. T. Kaczmarek, P. M. Ledingham, B. Brecht, S. E. Thomas, G. S. Thekkadath, O. Lazo-Arjona, J. H. D. Munns, E. Poem, A. Feizpour, D. J. Saunders, J. Nunn, and I. A. Walmsley, *Physical Review A* **97**, 042316 (2018).

<sup>37</sup>R. Finkelstein, E. Poem, O. Michel, O. Lahad, and O. Firstenberg, *Science Advances* **4**, eaap8598 (2018).

<sup>38</sup>F. Kaneda, K. Garay-Palmett, A. B. U'Ren, and P. G. Kwiat, *Optics Express* **24**, 10733 (2016).

<sup>39</sup>N. Montaut, L. Sansoni, E. Meyer-Scott, R. Ricken, V. Quiring, H. Herrmann, and C. Silberhorn, *Physical Review Applied* **8**, 024021 (2017).

<sup>40</sup>Y. J. Lu and Z. Y. Ou, *Phys. Rev. A* **62**, 033804 (2000).

<sup>41</sup>C. E. Kuklewicz, F. N. C. Wong, and J. H. Shapiro, *Phys. Rev. Lett.* **97**, 223601 (2006).

<sup>42</sup>Y. Jeronimo-Moreno, S. Rodriguez-Benavides, and A. B. U'Ren, *Laser Physics* **20**, 1221 (2010).

<sup>43</sup>J. A. Zielińska and M. W. Mitchell, *Optics Letters* **43**, 643 (2018).

<sup>44</sup>J. A. Zielińska, A. Zukauskas, C. Canalias, M. A. Noyan, and M. W. Mitchell, *Optics Express* **25**, 1142 (2017).

<sup>45</sup>M. Namazi, C. Kupchak, B. Jordaan, R. Shahrokhsahi, and E. Figueroa, *Physical Review Applied* **8**, 034023 (2017).

<sup>46</sup>B. Boulanger, M. M. Fejer, R. Blachman, and P. F. Bordui, *Applied Physics Letters* **65**, 2401 (1994), <https://doi.org/10.1063/1.112688>.

<sup>47</sup>O. B. Jensen, J. Holm, B. Sumpf, G. E. Peter, E. A. Paul, and M. Petersen, *Proc. SPIE 6455, Nonlinear Frequency Generation and Conversion: Materials, Devices, and Applications VI* **6455** (2007), 10.1117/12.700276.

<sup>48</sup>M. Minozzi, S. Bonora, A. V. Sergienko, G. Vallone, and P. Villoresi, *Optics Letters* **38**, 489 (2013).